

BeppoSAX spectroscopy of the NGC 7078 (M 15) globular cluster X-ray source X 2127+119

L. Sidoli, A.N. Parmar, and T. Oosterbroek

Astrophysics Division, Space Science Department of ESA, ESTEC, Postbus 299, NL-2200 AG Noordwijk, The Netherlands

Received 21 March 2000; Accepted: 20 June 2000

Abstract. Results of a 1999 November 16–17 BeppoSAX observation of the low-mass X-ray binary X 2127+119 located in the globular cluster M15 are presented. The system is believed to be one where the central neutron star is normally obscured by the accretion disk, and only X-rays scattered into our line of sight by an extended accretion disk corona (ADC) are observed. The 0.1–10 keV lightcurve is energy dependent and shows two partial eclipses separated by the 17.1 hr orbital period. The 0.1–100 keV spectrum is unusually complex, but can be successfully modeled using a partially covered power-law and disk-blackbody model. Together with a column consistent with the interstellar value to M15, $\sim 60\%$ of the source is covered by an additional column of $\sim 10^{22}$ atom cm^{-2} . The absorbed component may be X-rays that pass through the outer layers of the accretion disk. The energy dependent intensity variations by a factor of ~ 2 may be modeled as due to a changing normalization of the disk-blackbody. None of the other spectral parameters appear to clearly depend on luminosity. The same spectral model is also able to fit an archival ASCA spectrum. We demonstrate that during the luminous (\sim Eddington) X-ray burst observed from X 2127+119 by *Ginga*, material located in the outer regions of the accretion disk could have been temporarily ionized, so allowing the central neutron star to be viewed directly.

Key words: Accretion, accretion disks – Stars: individual: X 2127+119 – Stars: neutron – Globular cluster: individual: M15 (NGC 7078) – X-rays: general

1. Introduction

The X-ray source X 2127+119 is one of 12 bright ($L_x > 10^{36}$ erg s^{-1}) low-mass X-ray binaries (LMXBs) located within globular clusters. The X-ray source is located within $2''$ of the core of M15 (NGC 7078) and is coincident with the variable blue V ~ 15 star AC 211 (Aurière et al. 1984) which exhibits prominent optical and

UV emission and absorption lines (Charles et al. 1986; Downes et al. 1996). The optical lightcurve exhibits the largest amplitude variations of any LMXRB and is modulated with a period of 17.1 hr (Ilovaisky et al. 1993; hereafter I93). The X-ray lightcurve is weakly modulated with the same period, but shows a more complex behavior (see e.g., Homer & Charles 1998; hereafter HC98). The current model for the system consists of an X-ray binary viewed at a high inclination angle such that the central X-ray source is obscured by an accretion disk and only X-rays scattered into the line of sight by an extended accretion disk corona (ADC), or wind, are observed. This obscuration accounts for the low $L_x/L_{\text{opt}} \sim 20$ ratio for X 2127+119, typical of other ADC sources. Variations in the disk rim height and obscuration by the companion produce the observed modulation. The detection of a luminous (4.5×10^{38} erg s^{-1} at the peak, assuming isotropic emission) X-ray burst from X 2127+119 by *Ginga* confirms that the compact object is a neutron star and implies that, at times, the neutron star is viewed directly (Dotani et al. 1990; van Paradijs et al. 1990). The mean M15 metallicity is only ~ 0.01 solar (Geisler et al. 1992; Sneden et al. 1991) although this does not necessarily mean that the accreted material in the X 2127+119 system is strongly metal depleted since the companion star may have undergone a non-standard evolution during which its envelope composition was altered.

The X-ray spectrum of X 2127+119 is complex and varies on time scales shorter than the orbital period. Hertz & Grindlay (1983) combined data from the *Einstein* Monitor Proportional Counter (MPC) and High-Resolution Imager instruments and found that a two component model was required. One component is a thermal bremsstrahlung with a temperature, kT, of ~ 5 keV and the other appreciably softer. The source exhibited a strong anti-correlation between luminosity and absorption, N_H . The EXOSAT Channel Multiplier Array and Medium Energy Detector Array spectra of Callanan et al. (1987) are well fit by a two component model consisting of a ~ 1 keV blackbody together with a power-law with a photon index, α , of 1.6, or a blackbody with a similar kT together with a 7–15 keV thermal bremsstrahlung. The N_H was variable

in the range $0.15\text{--}3 \times 10^{21}$ atom cm^{-2} and showed a correlation with luminosity, in contrast to the result of Hertz & Grindlay (1983). Christian et al. (1997) present results from the *Einstein* Solid State Spectrometer and MPC instruments and the broadband X-ray telescope (BBXRT). They find that the continuum is well described by the same model used for the EXOSAT data (a power-law plus a 1 keV blackbody) with some evidence for the same anti-correlation as Hertz & Grindlay (1983). When the best-fit values of N_{H} are plotted against orbital phase, Φ , a factor ~ 10 increase in N_{H} is evident around $\Phi = 0.4\text{--}0.7$ (where $\Phi = 0.0$ corresponds to the center of the partial eclipse of the X-ray source by the companion star). If a spectral model with abundances fixed at the mean M15 value is used to model this extra absorption, then the fit is significantly poorer, with the model over-estimating the observed data at ~ 1.2 keV (see Christian et al. 1997, Fig. 5). No narrow Fe line is seen in the BBXRT data, with a 3σ upper limit of 150 eV.

We report here on a BeppoSAX observation of X 2127+119 made as part of a systematic study of luminous globular cluster X-ray sources (see Guainazzi et al. 2000 for an overview). Results for the sources located in Terzans 1 and 2 and NGC 6441 are to be found in Guainazzi et al. (1998, 1999) and Parmar et al. (1999), respectively. M15 has a low reddening ($E_{\text{B-V}} = 0.10 \pm 0.01$; Durrell & Harris 1993) which corresponds to $N_{\text{H}} \sim 7 \times 10^{20}$ atom cm^{-2} , using the relation between A_{V} and N_{H} in Predehl & Schmitt (1995). This low N_{H} means that the source is particularly interesting at energies $\lesssim 1$ keV. We compare the BeppoSAX results with an unpublished ASCA spectrum obtained in 1995. We note that EUV emission has been detected from M15 which may originate from X 2127+119 (Callanan et al. 1999).

2. Observations

Results from the co-aligned Low-Energy Concentrator Spectrometer (LECS; 0.1–10 keV; Parmar et al. 1997), the Medium-Energy Concentrator Spectrometer (MECS; 1.8–10 keV; Boella et al. 1997), and the Phoswich Detection System (PDS; 15–300 keV; Frontera et al. 1997) on-board BeppoSAX are presented. Due to technical reasons the HPGSPC was not operated. The MECS consists of two grazing incidence telescopes with imaging gas scintillation proportional counters in their focal planes. The LECS uses an identical concentrator system as the MECS, but utilizes an ultra-thin entrance window and a driftless configuration to extend the low-energy response to 0.1 keV. The non-imaging PDS consists of four independent units arranged in pairs each having a separate collimator. Each collimator was alternatively rocked on- and 210' off-source every 96 s during the observation.

The region of sky containing X 2127+119 was observed by BeppoSAX on 1999 November 16 01:15 to November 17 00:50 UTC. Good data were selected when the

instrument configurations were nominal, using the SAX-DAS 2.0.0 data analysis package. LECS and MECS data were extracted centered on the position of X 2127+119 using radii of 8' and 4', respectively. The exposures in the LECS, MECS, and PDS instruments are 11.1 ks, 35.5 ks, and 16.6 ks, respectively. Background subtraction for the imaging instruments was performed using standard files, but is not critical for such a bright source. Background subtraction for the PDS used data obtained during intervals when the collimators were offset from the source.

The BeppoSAX data is compared with results from the Solid State Imaging Spectrometers SIS0 and SIS1 (0.6–10 keV), on-board ASCA (Tanaka et al. 1994). ASCA observed X 2127+119 between 1995 May 16 00:54 and May 17 03:50 UTC. Timing results from this observation are reported in HC98. The SIS exposure is 25.0 ks using 1-CCD BRIGHT2 mode with the maximum available telemetry allocation. All data were screened and processed using the standard Rev2 pipeline. The source count rates of $\lesssim 9.0 \text{ s}^{-1}$ SIS $^{-1}$ mean that pulse pile-up is unlikely to be significant.

3. Analysis and results

3.1. BeppoSAX lightcurve

The BeppoSAX observation duration of 85 ks includes one entire orbital cycle of X 2127+119. Fig. 1 shows the 1.8–10 keV background subtracted MECS lightcurve of X 2127+119 with a binning time of 256 s. Fig. 2 shows background subtracted lightcurves in the energy ranges 0.1–2 keV (LECS), 1.8–5.5 keV (MECS), 5.5–10 keV (MECS) and 15–100 keV (PDS) together with hardness ratios (1.8–5.5 keV counts divided by 0.1–2 keV counts, and 5.5–10 keV counts divided by 1.8–5.5 keV counts). There is strong variability in the energy range 0.1–10 keV, with two deep minima separated by ~ 17 hr and a broad secondary minimum that occurred approximately midway between the two deep minima. The 3σ upper limit to any variability in the 15–100 keV PDS lightcurve ($\text{rms} < 0.61$) is consistent with the amount of variability seen at lower energies. The complex variations in hardness ratio suggest that it may be important to perform a spectral analysis in different source intensity ranges (see Sect. 3.3).

3.2. Eclipse timing

Recently HC98 refined the orbital ephemeris of I93 using results from all available X-ray lightcurves from HEAO-1 (1977) to R-XTE (1998). At the time of the BeppoSAX observation, the difference in Φ between the two ephemerides is ~ 0.05 . HC98 explained this difference either as an up-dated period of 0.713021 days (7σ larger than the I93 value of 0.713014 days), or by the introduction of a period derivative of $\dot{P}_{\text{orb}}/P_{\text{orb}} = 9 \times 10^{-7} \text{ yr}^{-1}$. Fig. 3 shows lightcurves in different energy bands plotted

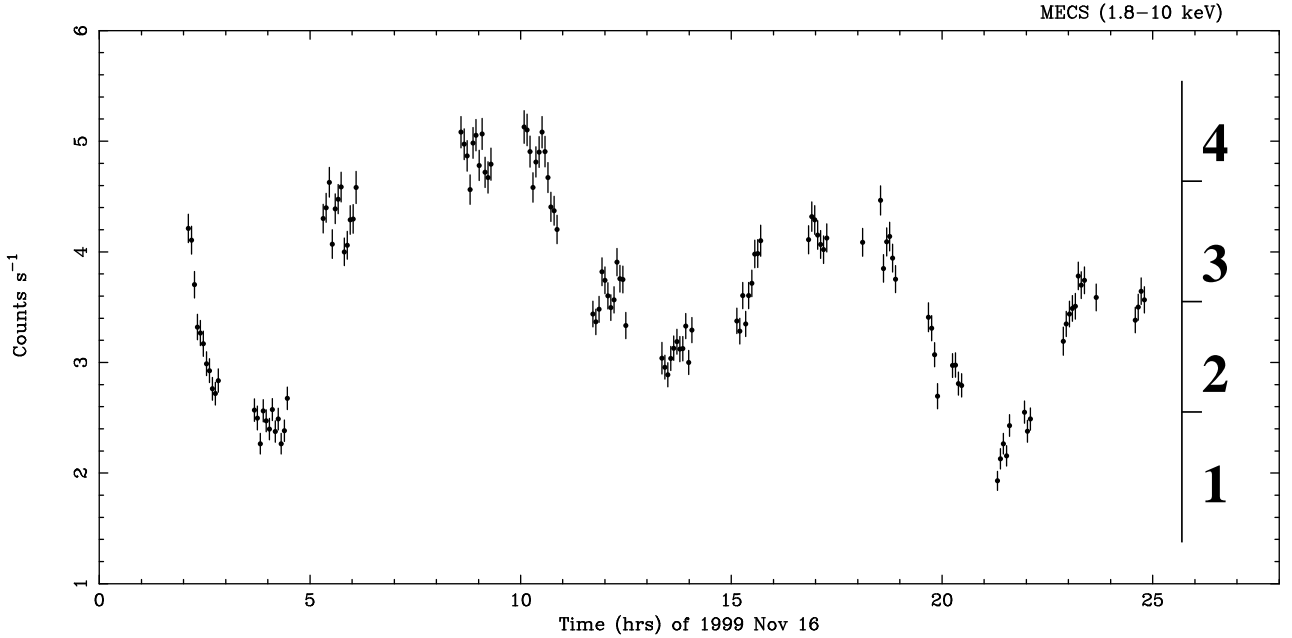


Fig. 1. The 1.8–10 keV lightcurve of X 2127+119. The 4 intensity intervals used in the spectral analysis (see Sect. 3.3.2) are indicated. The bin time is 256 s

against Φ using the HC98 linear ephemeris. There is good agreement between the BeppoSAX data and the refined ephemeris. In order to investigate whether the BeppoSAX data can be used to further refine the ephemeris we performed a detailed timing analysis.

The occurrence time of the first minimum in the BeppoSAX lightcurve is $2,451,498.6614 \pm 0.0044$ JD $_{\odot}$, which corresponds to cycle 5200 using the I93 epoch. This eclipse time was calculated by folding the 1.8–10 keV MECS data at the HC98 linear ephemeris and selecting an interval of 0.2 in phase around the partial eclipse. A fit with a model consisting of a constant plus a gaussian was made to this data. The uncertainty in the eclipse time was obtained from $\Delta\chi^2=1.0$ after scaling the errors such that χ^2_{ν} was ~ 1 . The partial eclipse arrival time extrapolated to cycle 5200 starting from this same epoch, but using the new HC98 period of 0.713021 days is $2,451,498.6774 \pm 0.023$ (JD $_{\odot}$), a difference of 0.016 ± 0.023 days. Note that, since HC98 and I93 apparently did not apply a barycentric correction, we have included this correction (which is however much smaller than the uncertainties). Using the quadratic ephemeris of HC98 (for which the difference with respect to the I93 ephemeris is estimated from HC98 Fig. 2 and amounts to ~ 0.07 cycle) we obtain an expected occurrence time of $2,451,498.691 \pm 0.03$ JD $_{\odot}$, a difference of 0.03 ± 0.03 days. Similarly, the predicted partial eclipse center using the original I93 ephemeris is $2,451,498.6410 \pm 0.023$ (JD $_{\odot}$), resulting in a difference of 0.020 ± 0.023 days.

Thus, our measure of the partial eclipse occurrence is in agreement with the 3 previously published ephemerides and does not allow us to distinguish between them.

3.3. BeppoSAX spectrum

3.3.1. Overall spectrum

The overall spectrum of X 2127+119 was first investigated by simultaneously fitting data from the LECS, MECS and PDS using XSPEC version 11.01. All spectra were rebinned using standard procedures. Data were selected in the energy ranges 0.1–4.0 keV (LECS), 1.8–10 keV (MECS), and 15–100 keV (PDS) where the instrument responses are well determined and sufficient counts obtained. This gives background-subtracted count rates of 2.1, 3.7, and 1.0 s $^{-1}$ for the LECS, MECS, and PDS, respectively. The photoelectric absorption cross sections of Morrison & McCammon (1983) and the abundances of Anders & Grevesse (1989) are used throughout. Factors were included in the spectral fitting to allow for normalization uncertainties between the instruments. These factors were constrained to be within their usual ranges during the fitting. All spectral uncertainties and upper-limits are given at 90% confidence.

Initially, simple models were tried, including absorbed power-law, thermal bremsstrahlung and cutoff power-law models, all yielding unacceptable results for the broad band spectrum. When a power-law model is used, examination of the residuals shows a curved spectrum in the energy range 2–10 keV and a structured soft excess below about 1 keV. Several different combinations of spectral model were tried next, always including a power-law, which is required by the PDS data. Both a blackbody and a bremsstrahlung were added to the power-law in order to account for the curvature of the 2–10 keV spectrum,

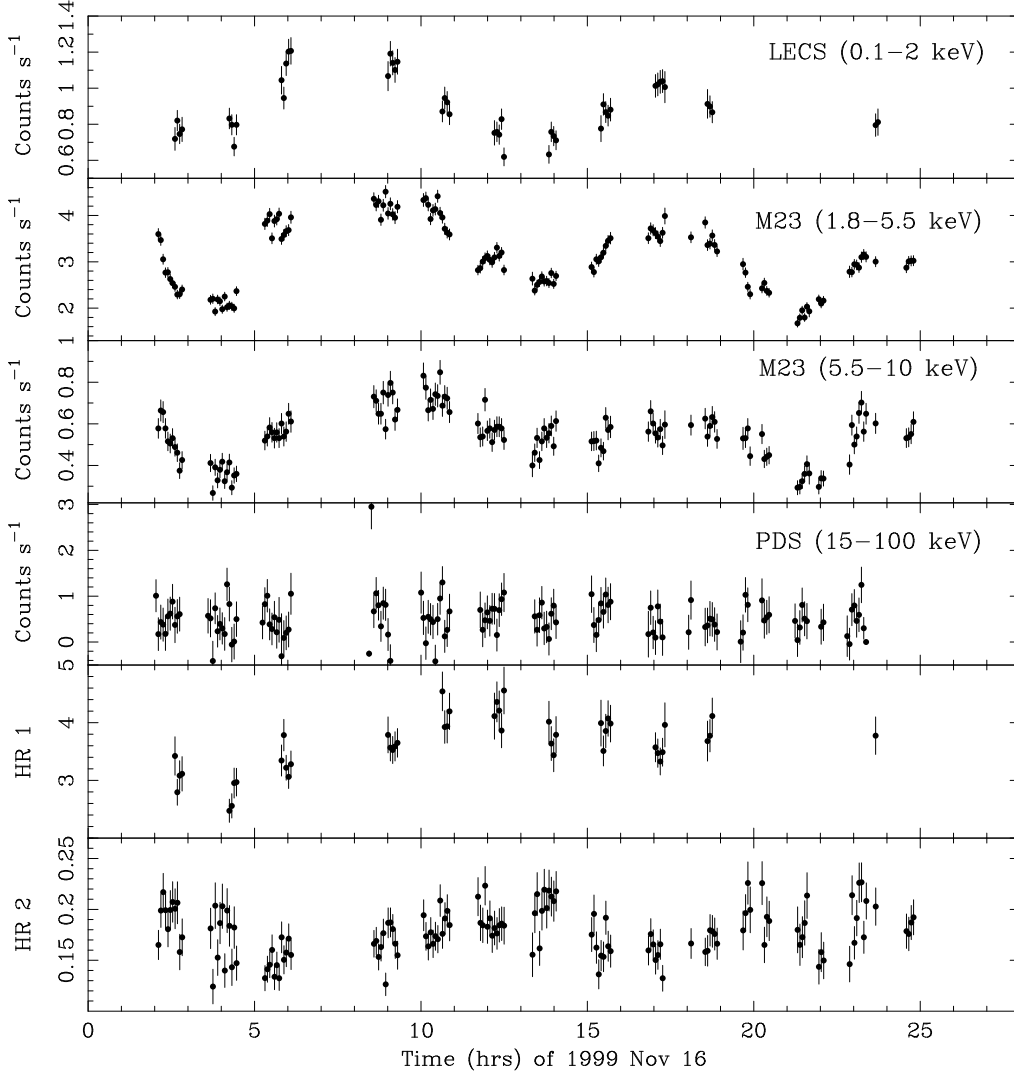


Fig. 2. X 2127+119 lightcurves in different energy bands and hardness ratios (lower 2 panels). HR1 is MECS 1.8–5.5 keV counts / LECS 0.1–2 keV counts and HR2 MECS 5.5–10 keV counts / MECS 1.8–5.5 keV counts. The bin time is 256 s

but always gave unacceptable results, primarily due to the structured residuals below 1 keV.

An absorbed ($N_H \sim 10^{21}$ atom cm^{-2}) multicolour disk-blackbody (the DISKBB model in XSPEC) (with $kT_{\text{in}} \sim 1.8$ keV) together with an absorbed power-law with $\alpha \sim 1.7$ gives significantly better results, but again low-energy residuals are present. The multicolour disk-blackbody model of Mitsuda et al. (1984) and Makishima et al. (1986) assumes that the gravitational energy released by the accreting material is locally dissipated into blackbody radiation, that the accretion flow is continuous throughout the disk and that the effects of electron scattering on the spectrum are negligible. There are only two parameters in the model: $R_{\text{in}}(\cos\theta)^{0.5}/d_{10}$ where R_{in} is the innermost radius of the disk, θ the inclination angle of the disk, d_{10} the source distance in units of 10 kpc,

and kT_{in} the blackbody effective temperature at R_{in} . The limitations of this model are discussed in Merloni et al. (2000).

The low metallicity of the hosting globular cluster (~ 0.01 solar) prompted us to try using a photoelectric absorption model with variable abundances (VPHABS in XSPEC), together with a photoelectric absorption fixed at the interstellar value of 7×10^{20} atom cm^{-2} . Different combinations of linked abundances were tried. First, fixing the He abundance at the cosmic value and linking all the abundances of the metals together as a single parameter. Then, linking C, N and O together and grouping the other metals (Ne, Na, Mg, Al, Si, S, Cl, Ar, Ca, Cr, Fe, Co, Ni) as another parameter, both fixing the abundance of the metals at 0.01 of the solar value and letting it vary freely. In all cases unacceptable results are obtained. No

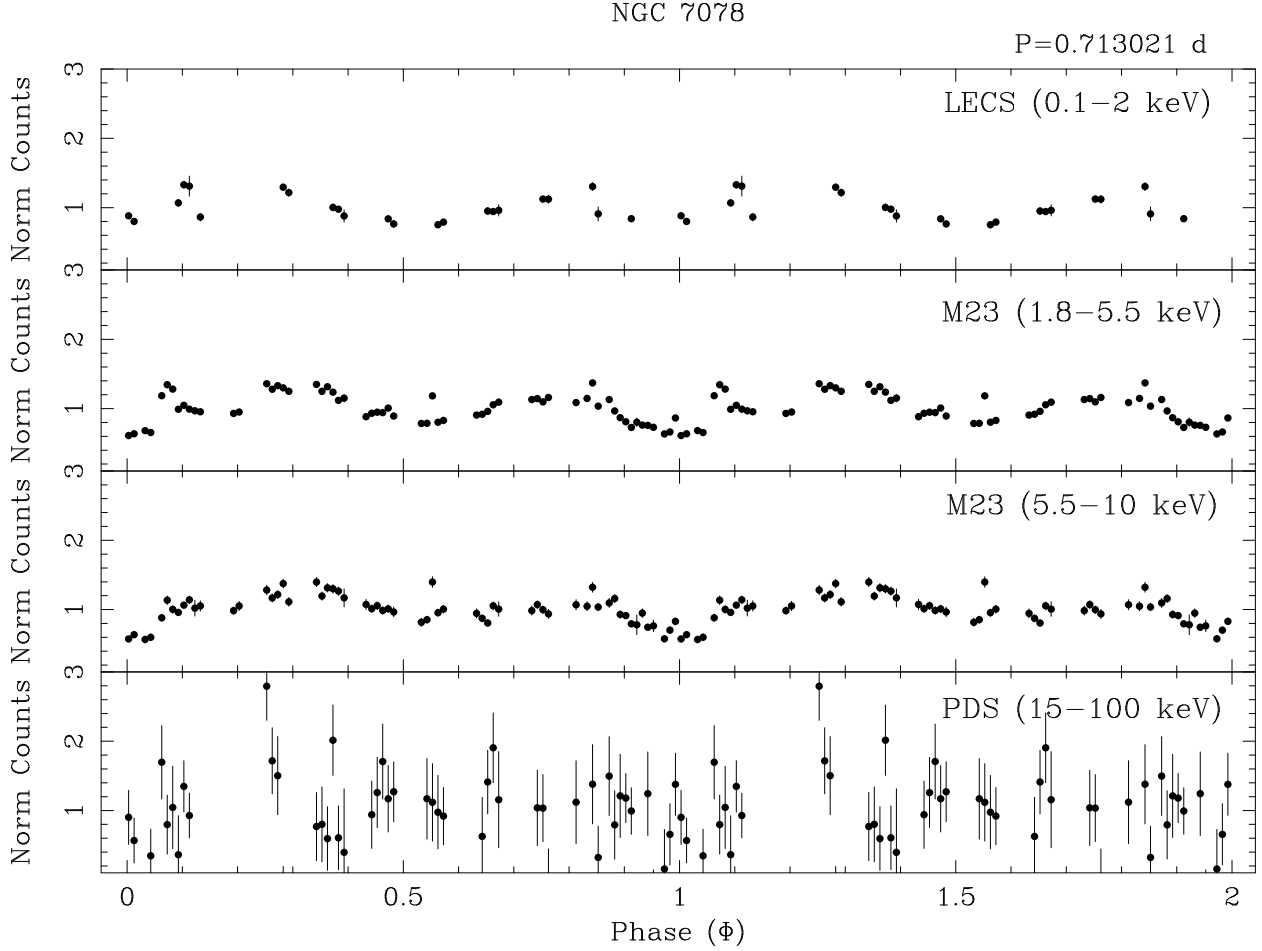


Fig. 3. X 2127+119 lightcurves scaled to show the same range of variability

K_{α} iron line is present with a 90% confidence upper limit to the equivalent width of a narrow line of 50 eV.

The positive residuals below 1 keV suggest the presence of either (1) partial covering, (2) an ionized absorber or (3) an additional soft component. Thus, we first used the same model as before (a power-law plus a disk-blackbody), but allowed the absorption of each component to vary separately, while being constrained to be not less than the galactic value. Significantly better fits were obtained when the disk-blackbody suffered extra absorption, and so the absorption of the power-law component was set equal to the galactic value, N_{gal} ($7 \times 10^{20} \text{ atom cm}^{-2}$). The model can be written as follows:

$$\text{Intensity} = e^{-\sigma N_{\text{gal}}} (I_{\text{DBB}} e^{-\sigma N_{\text{H}}} + I_{\text{PL}}),$$

where I_{DBB} and I_{PL} are the normalizations of the disk-blackbody and power-law components, and N_{H} is the additional column density of the disk-blackbody. The best-fit values are $N_{\text{H}} = (7.0^{+1.00}_{-0.60}) \times 10^{21} \text{ atom cm}^{-2}$, $kT_{\text{in}} = 1.72^{+0.04}_{-0.03} \text{ keV}$, $R_{\text{in}}(\cos \theta)^{0.5}/d_{10 \text{ kpc}} = 1.2 \pm 0.05 \text{ km}$, $\alpha = 1.84 \pm 0.05$. Although the fit is not formally acceptable with a χ^2 of 177 for 125 degrees of freedom (dof), the

overall shape of the spectrum is reasonably well accounted for by this model.

A significantly better fit is obtained if a partial covering absorption (the PCFABS model in XSPEC) replaces the different absorbing column for the two components. This model consists of a column density fixed at the galactic value, together with partial covering absorption for the previous two components (a disk-blackbody and a power-law):

$$\text{Intensity} = e^{-\sigma N_{\text{gal}}} [f e^{-\sigma N_{\text{H}}} + (1 - f)] (I_{\text{DBB}} + I_{\text{PL}}),$$

where N_{H} is the intrinsic absorption for both spectral components and f is the covering fraction ($0 < f < 1$). The χ^2 is significantly reduced to 147.5 for 125 dof. The count and photon spectra are shown in Fig. 4 and the best-fit parameters given in Table 1.

In order to test the second possibility, we replaced the partial covering absorption with an ionized absorber (ABSORI in XSPEC) in our best fit model. The new model resulted in a worse fit, both when the iron abundance was fixed at the M15 value ($\chi^2 = 176.6$ for 125 dof and an ionization parameter $L/nR^2 = 40 \pm 20$) and when fixed at

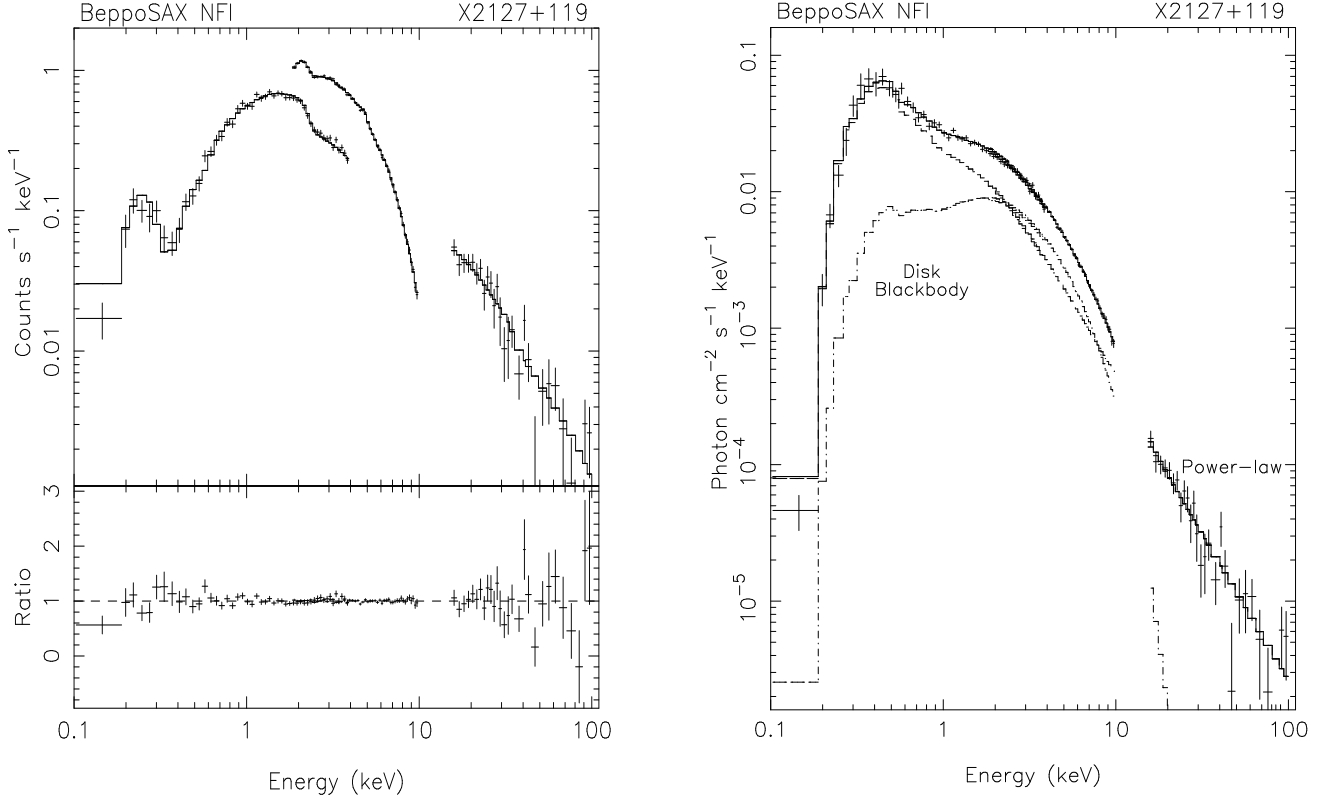


Fig. 4. Best-fit partial covering model to the BeppoSAX broad band spectrum of X 2127+119. See Table 1 for the parameters

the solar value ($\chi^2 = 166.3$ for 125 dof and an ionization parameter of 17 ± 10).

The final possibility is the presence of an additional soft component. To test this hypothesis, we included a bremsstrahlung ($T \sim 0.1$ keV), a blackbody, and a broad Gaussian line to the disk-blackbody and power-law model. None of these additional components significantly improved the fit, giving values of χ^2/dof of 229/124, 890/127 and 245/123, respectively. Thus, we exclude the possibility that the low-energy residuals are caused by such an additional component. We therefore conclude that of the models tried, the partial covering gives the most reasonable fit and we refer to this subsequently as the best-fit model. The lower limit to any high energy cutoff is 60 keV at 90% confidence level. Since Fig. 2 indicates that there are strong energy dependent intensity variations, we next investigated whether the best-fit model could be successfully applied to individual intensity selected spectra.

3.3.2. Intensity selected spectra

A series of intensity selected spectra were produced. Intervals corresponding to MECS 1.8–10 keV count rates of <2.6 , 2.6–3.6, 3.6–4.6, and >4.6 s $^{-1}$, when the data are accumulated with a binning of 256 s, were determined (see Fig. 1). These intervals were used to extract a set of

Table 1. Best-fit parameters for the overall BeppoSAX spectrum. The model consists of a partial covering (PC-FABS) absorption, N_H , for a DISKBB and a power-law (see text). Flux is in the 2–10 keV energy range and in units of erg cm $^{-2}$ s $^{-1}$. The luminosity (2–10 keV) has been corrected for interstellar absorption and assumes a distance of 10.4 kpc (Durrel & Harris 1993)

Parameter	
N_{gal} (10^{20} atom cm $^{-2}$)	7 (fixed)
N_H (10^{22} atom cm $^{-2}$)	$1.03^{+0.12}_{-0.09}$
f	$0.64^{+0.05}_{-0.04}$
kT_{in} (keV)	$1.77^{+0.09}_{-0.07}$
$R_{\text{in}}(\cos \theta)^{0.5}/d_{10}$ (km)	1.03 ± 0.05
α	2.10 ± 0.10
I_{PL}	0.063 ± 0.01
Observed Flux	2.7×10^{-10}
Luminosity (erg s $^{-1}$)	3.3×10^{36}
χ^2/dof	147.5/125

four corresponding LECS, MECS and PDS spectra which were rebinned and energy selected in the same way as in Sect. 3.3.1. The different intensity ranges correspond ap-

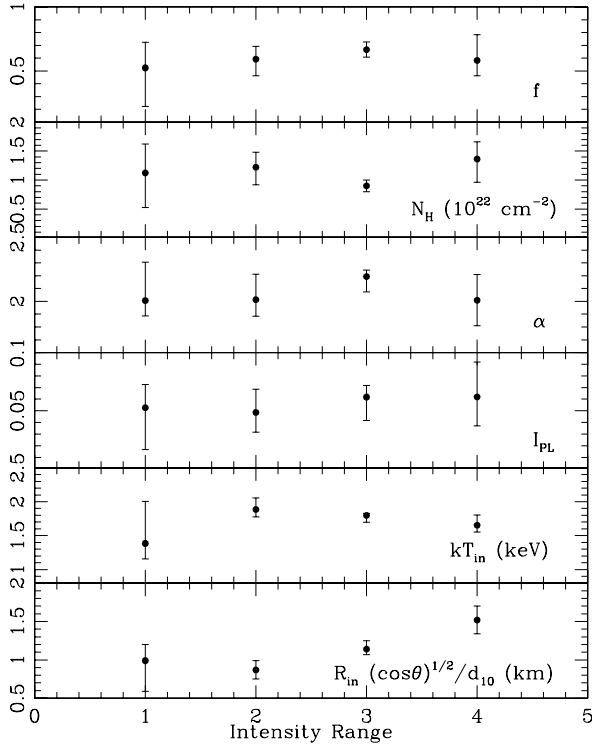


Fig. 5. Variation of the best-fit spectral parameters with intensity (see Table 2)

proximately to the deepest minimum (1), the broad secondary minimum (2), the secondary maximum (3) and the brightest first maximum (4). Since the power-law and disk-blackbody with a partial covering absorption provides the best-fit to the overall spectrum, this model was also fit to these new spectra. Acceptable fits are also obtained in this case and the results reported in Table 2 and Fig. 5.

Examination of the parameters given in Table 2 shows that N_H , f , kT_{in} , α , and I_{PL} do not vary systematically with luminosity, but that the normalization of the disk-blackbody ($R_{in}(\cos\theta)^{0.5}/d_{10}$) increases significantly with increasing luminosity. See Fig. 5 for the dependence of the spectral parameters on intensity. The disk-blackbody component contributes between 24% and 62% of the observed flux (uncorrected for the interstellar absorption) in the 2–10 keV energy range. Thus, the energy dependent variations shown in Figs. 2 and 3 may be largely explained by variations in the normalization of this component.

3.3.3. Phase selected spectra

In order to investigate the spectral variation as a function of Φ , four sets of phase selected spectra were extracted and fit with the best-fit model. The results, shown in Fig. 6, may be compared with the variations in spectral parameters with intensity shown in Fig. 5. The four sets of spectra correspond to primary minimum, primary maximum, secondary minimum and secondary maximum, respectively.

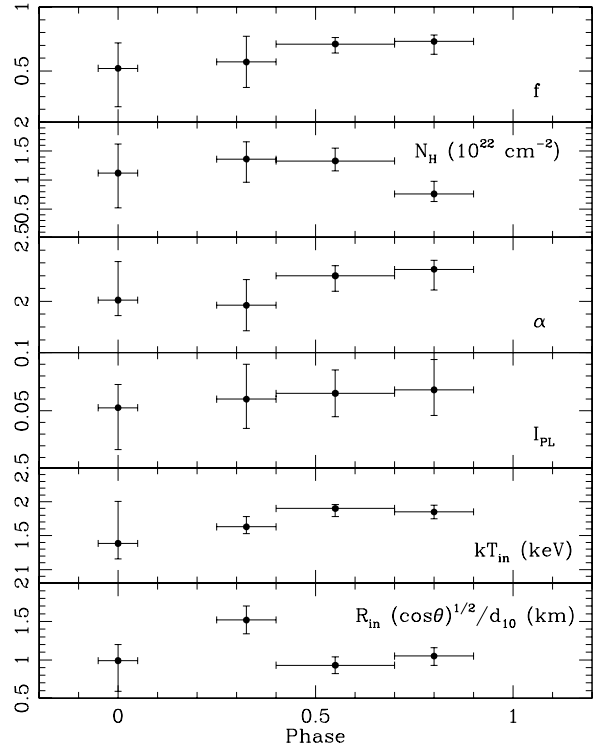


Fig. 6. Variation of the best-fit spectral parameters with orbital phase

The column density does not display any obvious dependence on Φ , except possibly when the source is in the secondary maximum. As expected, the disk-blackbody normalization exhibits the most obvious dependence on Φ , showing a similar correlation to that with source intensity.

3.4. ASCA spectrum

We next examined whether the BeppoSAX best-fit model presented above is consistent with results from ASCA. The best-fit BeppoSAX model was fit to the SIS spectra (see Fig. 7) and the results are presented in Table 3. We only considered data above 1 keV due to SIS calibration uncertainties at lower energies (Hwang et al. 1999). Our results show that the best-fit BeppoSAX model also provides a good fit to the ASCA SIS spectra giving a χ^2 of 912.0 for 848 dof. This is a significantly better fit than when an absorbed disk-blackbody plus a power-law model is used which gives a χ^2 of 1034 for 849 dof. During the ASCA observation the 2–10 keV flux uncorrected for interstellar absorption was 3.0×10^{-10} erg cm $^{-2}$ s $^{-1}$, within 10% of the value during the BeppoSAX observation, and the disk-blackbody contributed 32% of the total observed flux in this energy range.

Table 2. Best-fits to the BeppoSAX NFI spectra in intensity intervals 1 to 4. The model consists of a partial covering (PCFABS) absorption, N_H , for a DISKBB and a power-law (see text). Fluxes are in the 2–10 keV energy range and in units of 10^{-10} erg cm $^{-2}$ s $^{-1}$. Luminosities (2–10 keV) are in units of 10^{36} erg s $^{-1}$ and are corrected for interstellar absorption and assume a distance of 10.4 kpc. f_{bb} is the fraction of the total observed flux contributed by the disk-blackbody component in the energy range 2–10 keV

Parameter	1	2	3	4
N_H (10^{22} atom cm $^{-2}$)	$1.12^{+0.50}_{-0.60}$	1.22 ± 0.3	0.90 ± 0.1	$1.36^{+0.3}_{-0.4}$
f	$0.52^{+0.2}_{-0.3}$	$0.59^{+0.10}_{-0.13}$	0.67 ± 0.06	0.57 ± 0.2
kT_{in} (keV)	$1.39^{+0.62}_{-0.23}$	$1.89^{+0.17}_{-0.11}$	$1.80^{+0.03}_{-0.1}$	$1.63^{+0.15}_{-0.10}$
$R_{in}(\cos \theta)^{0.5}/d_{10}$ (km)	$0.99^{+0.21}_{-0.40}$	0.87 ± 0.12	$1.14^{+0.11}_{-0.07}$	1.52 ± 0.18
α	$2.01^{+0.3}_{-0.12}$	$2.01^{+0.2}_{-0.13}$	$2.19^{+0.05}_{-0.12}$	1.97 ± 0.2
I_{PL}	$0.053^{+0.020}_{-0.036}$	0.049 ± 0.020	0.062 ± 0.020	0.060 ± 0.030
Observed Flux	1.7	2.4	2.9	3.5
Luminosity	2.1	3.0	3.6	4.4
f_{bb}	0.24	0.53	0.62	0.60
χ^2/dof	137.9/113	138/117	128/121	114.8/115

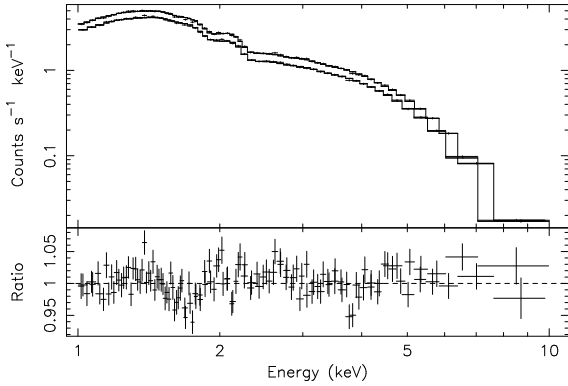


Fig. 7. Best-fit model to the ASCA-SIS spectrum of X 2127+119. See Table 3 for the parameters

4. Discussion

We present results of a 1999 November BeppoSAX observation of X 2127+119 covering two partial eclipses and compare these with an earlier ASCA observation when the source had a similar 2–10 keV intensity. The decrease in the 0.1–10 keV flux during the partial eclipses is smooth and gradual and lasts for at least 0.2 in phase and the secondary minimum at $\Phi \sim 0.5$ is broader than the primary minima. The overall variation in the hardness ratios HR1 and HR2 reveals a complex behaviour, with a large change of the HR1 during the partial eclipses. In particular, no spectral softening with increasing intensity is found, contrary to the EXOSAT results of Callanan et al. (1987).

The 0.1–100 keV BeppoSAX spectrum is unusually complex and cannot be fit by any of the usual models applied to LMXRB such as an absorbed power-law and a blackbody. A good fit is obtained with the combination of a power-law and a disk-blackbody modified by a partial covering absorption (with additional absorption fixed

Table 3. Best-fit parameters for the overall ASCA spectrum. The model consists of a partial covering (PCFABS) absorption, N_H , for a DISKBB and a power-law (see text). Flux is in the 2–10 keV energy range and in units of erg cm $^{-2}$ s $^{-1}$. The luminosity (2–10 keV) has been corrected for interstellar absorption and assumes a distance of 10.4 kpc

Parameter	
N_{gal} (10^{20} atom cm $^{-2}$)	7 (fixed)
N_H (10^{22} atom cm $^{-2}$)	0.86 ± 0.20
f	0.76 ± 0.03
kT_{in} (keV)	$1.96^{+0.20}_{-0.10}$
$R_{in}(\cos \theta)^{0.5}/d_{10}$ (km)	0.70 ± 0.12
α	$2.18^{+0.15}_{-0.21}$
I_{PL}	$0.11^{+0.02}_{-0.03}$
Observed Flux	3.0×10^{-10}
Luminosity	3.7×10^{36}
χ^2/dof	912/848

at the interstellar value). The same model provides a reasonable fit to an ASCA SIS spectrum obtained in 1995. We have divided the BeppoSAX data into 4 intensity selected intervals and fit the above best-fit model to these data. We find a positive correlation between the disk-blackbody normalization and the source intensity with the disk-blackbody contributing between 24% and 62% of the total 2–10 keV flux. The absorption, the blackbody kT , α , and the power-law normalization do not vary systematically as the 2–10 keV source intensity varies by a factor ~ 2 .

A phase selected spectral analysis also shows a correlation of the disk-blackbody normalization with source

intensity (see Fig. 6, bottom panel). The variability of the disk-blackbody component dominates the overall intensity and hardness variations of the source. The variation in hardness ratio HR1 during the partial eclipse is better modeled by a variation in the contribution of the disk-blackbody component. The absorbing column density remains constant (within uncertainties) during and after the partial eclipse (Fig. 6).

The secondary minimum is one of the most variable and puzzling feature of this source. Its location at $\Phi \sim 0.5$ is difficult to explain in terms of material located in a bulge formed by the impact of an accretion stream with the outer edge of the disk since this is usually located at $\Phi \sim 0.8$ (see e.g., White & Holt 1982; Mason & Cordova 1982). I93 and Christian et al. (1997) suggest that the secondary minimum is due to obscuring material located in a ring at the circularization radius in the accretion disk, as in the model by Frank et al. (1987). However, we find no evidence for a higher N_H during the secondary minimum (see Fig. 6). We caution however, that the complex low-energy X 2127+119 spectrum makes the detailed interpretation of any spectral changes difficult.

It is interesting to speculate as to the physical nature of the different components required to fit the X 2127+119 spectrum. The disk-blackbody component is most likely emission from the inner regions of the accretion disk and/or from a boundary layer (see e.g., Popham & Sunyaev 2000). This emission is then scattered into the line of sight by the extended ADC. The power-law component is usually interpreted as being due to the Comptonization of soft photons by hot electrons located in the ADC. In this case, the photon index translates into a Comptonization y parameter of ~ 0.7 . This non-thermal component does not show any evidence for a cut-off, with a lower limit of 60 keV, indicating that the electron temperature must be $\gtrsim 20$ keV.

It is interesting to note that the ADC source X 1822–371 has also a very complex X-ray spectrum. If the BeppoSAX and ASCA spectra are fit with simple power-law model then a strong deficit is visible at ~ 1.5 keV. This may be modeled as an edge at ~ 1.3 keV together with the intersection of power-law and blackbody components (Parmar et al. 2000). There is also low-energy complexity in the X 2127+119 spectrum (see Fig. 4), but no edge is required. This difference may be related to the low abundance appropriate to X 2127+119. It is surprising that the intensities of the two spectral components in X 2127+119 do not vary in the same way in the intensity selected fits. This would be the case if the modulation was simply caused by the geometric obscuration of a homogeneously emitting ADC. The fact that the power-law normalization during the partial eclipses is perfectly consistent (within the uncertainties) with the values outside the partial eclipses (see Fig. 5), implies that the region emitting this component is significantly larger than the companion star. On the other hand, we note that the uncer-

tainties on the power-law normalizations are large and an obscuration of an homogeneously emitting ADC by a factor of ~ 3 during the partial eclipse by the companion star (with the estimated dimensions) would be undetectable as a decrease of this same factor in the power-law normalization (within the uncertainties).

The nature of the absorbed component required in both the BeppoSAX and ASCA spectral fits is uncertain. One possibility is that this is emission that passes through structure at the outer edge of the accretion disk after first being scattered in the ADC. Rather than a single value of N_H , the measured value would then represent an average, since a range of absorbing columns would be expected in this case.

The orbital period $P=17.11$ hr implies the presence of a (sub)giant companion (e.g., Verbunt & Van den Heuvel 1995). The parameters of the binary system can be derived from the orbital period P_{orb} and assuming the mass ratio, q , between the mass of the companion M_c and the mass of the neutron star M_{ns} . Taking $M_c = 0.8 M_\odot$ (the typical mass for a turn-off star in a globular cluster) and $M_{\text{ns}} = 1.4 M_\odot$, the binary separation is $a = 3 \times 10^{11}$ cm, the radius R_c of the companion star, filling the Roche lobe, is $R_c \sim 10^{11}$ cm, the disk radius is $R_{\text{disk}} \sim 10^{11}$ cm, the diameter of the extended X-ray source (ADC) is $\sim 1.5 \times 10^{11}$ cm (I93).

The nature of X 2127+119 is intriguing. The fact that X 2127+119 contains a neutron star was firmly established by the detection of a radius expansion X-ray burst during a *Ginga* observation in 1988 (Dotani et al. 1990, van Paradijs et al. 1990). Although the *Ginga* Large Area Counter has a large field of view ($0.8^\circ \times 1.7^\circ$), it is clear that the burst came from X 2127+119 since there was no other known X-ray source in the field of view and between the precursor and the main peak of the burst there was a significant reduction in the persistent X-ray flux. Thus the burst must almost certainly have come from the source of the persistent emission, X 2127+119. The detection of such a luminous (4.5×10^{38} erg s $^{-1}$ at the peak, assuming isotropic emission) burst indicates that at times the surface of the neutron star is directly observed. The evidence that X 2127+119 is primarily an ADC source comes mainly from the extremely low L_x/L_{opt} ratio, typical of other ADC sources, the partial X-ray eclipses and the optical spectrum which resembles that of other ADC sources (e.g., Downes et al. 1996).

This apparently discrepant nature could be resolved if the highly energetic burst ionized the absorbing material in the line of sight, as proposed by Smale et al. (1992) for an X-ray burst observed from the dipping LMXRB X 1916–053. Following Smale et al. (1992), the number of photons per unit area emitted by the burst and available to ionize the obscuring material can be calculated from $N_{\text{ph}} = L\Delta t / \epsilon 4\pi R^2$, where L is the luminosity of the burst, Δt the duration of the most luminous part of the burst, ϵ is the mean X-ray energy, and R the distance of the obscur-

ing material to the source. Taking $L \sim 10^{38}$ ergs s $^{-1}$, $\Delta t \sim 1$ s, $\epsilon \sim 1$ keV, and $R \sim 10^{11}$ cm, gives $N_{\text{ph}} \sim 5 \times 10^{23}$ photons cm $^{-2}$, a hundred times larger than the intrinsic column density determined here. So, material located in the outer regions of the accretion disk could have been temporarily ionized, allowing the neutron star to be viewed directly.

Acknowledgements. The BeppoSAX satellite is a joint Italian-Dutch programme. L. Sidoli acknowledges an ESA Fellowship. This research has made use of data obtained through the High Energy Astrophysics Science Archive Research Center Online Service, provided by the NASA/Goddard Space Flight Center.

References

- Anders E., Grevesse N., 1989, *Geochimica et Cosmochimica Acta* 53, 197
- Aurière M., le Fèvre O., Terzan A., 1984, *A&A* 138, 415
- Boella G., Chiappetti L., Conti G., et al., 1997, *A&AS* 122, 327
- Callanan P.J., Fabian A.C., Tennant A.F., Redfern R.M., Shafer R.A., 1987, *MNRAS* 224, 781
- Callanan P.J., Drake J.J., Fruscione A., 1999, *ApJ* 521, 125
- Charles P.A., Jones D.C., Naylor T., 1986, *Nat* 323, 417
- Christian D.J., Smale A.P., Swank J.H., Serlmitos P.J., 1997, *ApJ* 477, 424
- Dotani T., Inoue H., Murakami T., et al., 1990, *Nat* 347, 534
- Downes R.A., Anderson S.F., Margon B., 1996, *PASP* 108, 688
- Durrell P.R., Harris W.E., 1993, *AJ* 105, 1420
- Frank J., King A.R., Lasota J.P., 1987, *A&A* 178, 137
- Frontera F., Costa E., Dal Fiume D., et al., 1997, *A&AS* 122, 371
- Geisler D., Minniti D., Claria J., 1992, *AJ* 104, 627
- Guainazzi M., Parmar A.N., Segreto A., Stella L., Oosterbroek T., 1998, *A&A* 339, 802
- Guainazzi M., Parmar A.N., Oosterbroek T., 1999, *A&A* 349, 819
- Guainazzi M., Parmar A.N., Oosterbroek T., 2000, *Ap. Lett & Comm.* submitted
- Hertz P., Grindlay J.E., 1983, *ApJ* 275, 105
- Homer L., Charles P.A., 1998, *New Astron.* 7, 435 (HC98)
- Hwang U., Mushotzky R.F., Burns J.O., et al., 1999, *ApJ* 516, 604
- Ilovaisky S.A., Chevalier C., Aurière M., et al., 1993, *A&A* 270, 139 (I93)
- Makishima K., Maejima Y., Mitsuda K., et al., 1986, *ApJ* 285, 712
- Mason K.O., Cordova F.A., 1982, *ApJ* 262, 253
- Merloni A., Fabian A.C., Ross R.R., 2000, *MNRAS* 313, 193
- Mitsuda K., Inoue H., Koyama K., et al., 1984, *PASJ* 36, 741
- Morrison D., McCammon D., 1983, *ApJ* 270, 119
- Parmar A.N., Martin D.D.E., Bavdaz M., et al., 1997, *A&AS* 122, 309
- Parmar A.N., Oosterbroek T., Guainazzi M., et al., 1999, *A&A* 351, 225
- Parmar A.N., Oosterbroek T., Del Sordo S., et al., 2000, *A&A* 356, 175
- Popham R., Sunyaev R., 2000, preprint (astro-ph/0004017), *ApJ* submitted
- Predehl P., Schmitt J.H.M.M., 1995, *A&A* 293, 889
- Smale A.P., Mukai K., Williams O.R., Jones M.H., Corbet R.H.D., 1992, *ApJ* 400, 330
- Snedden C., Kraft R.P., Prosser C.F., Langer G.E., 1991, *AJ* 102, 2001
- Tanaka Y., Inoue H., Holt S.S., 1994, *PASP* 46, L37
- Van Paradijs J., Dotani T., Tanaka Y., Tsuru T., 1990, *PASJ* 42, 633
- Verbunt F., van den Heuvel E.P.J., 1995, in “X-ray Binaries”, Lewin W.H.G., van Paradijs J., van den Heuvel E.P.J. eds., Cambridge Univ. Press, Cambridge, p. 457
- White N.E., Holt S.S., 1982, *ApJ* 257, 318